Journal Name

ARTICLE TYPE

Cite this: DOI: 00.0000/xxxxxxxxxx

Discovery of Superconductivity in Nb_4SiSb_2 with a V_4SiSb_2-Type Structure and Implications of Interstitial Doping on its Physical Properties

Manuele D. Balestra,[ab] Omargeldi Atanov [c], Robin Lefèvre,[b] Olivier Blacque,[b] Yat Hei Ng,[c] Rolf Lortz,[c] Fabian O. von Rohr[a*]

Received Date
Accepted Date

DOI: 00.0000/xxxxxxxxxx

We report on the discovery, structural analysis, and the physical properties of Nb_4SiSb_2 – a *hitherto* unknown compound crystallizing in the V_4SiSb_2-type structure with the tetragonal space group *I4/mcm* and unit cell parameters $a = 10.3638(2)$ Å and $c = 4.9151(2)$ Å. We find Nb_4SiSb_2 to be a metal undergoing a transition to a superconducting state at a critical temperature of $T_c \approx 1.6$ K. The bulk nature of the superconductivity in this material is confirmed by the observation of a well defined discontinuity in specific heat with a normalized specific heat jump of $\Delta C(T_c)/\gamma T_c = 1.33\,\mathrm{J\,mol^{-1}\,K^{-2}}$. We find that for Nb_4SiSb_2, the unoccupied sites on the 4*b Wyckoff* position can be partially occupied with Cu, Pd, or Pt. Low-temperature resistivity measurements show transitions to superconductivity for all three compounds at $T_c \approx 1.2\,\mathrm{K}$ for $Nb_4Cu_{0.2}SiSb_2$, and $T_c \approx 0.8\,\mathrm{K}$ for $Nb_4Pd_{0.2}SiSb_2$ as well as for $Nb_4Pt_{0.14}SiSb_2$. The addition of electron-donor atoms into these void positions, henceforth, lowers the superconducting transition temperature in comparison to the parent compound.

1 Introduction

A promising approach for the discovery of new superconducting materials is based on the substitution or incorporation of elements into existing structures with crystallographic void positions. Substituting or incorporating atoms into a structure allows for the precise chemical modification of the density of electronic states at the Fermi-level. This may induce superconductivity or tune superconducting properties.[1–5] Recent examples of this include the increase in the superconducting transition temperature of Nb_5Ge_3 – in the tetragonal Cr_5B_3 type-structure – from $T_c \approx 0.7\,\mathrm{K}$ to 15.3 K by the incorporation of carbon atoms into void positions,[6] or the stabilization of η-carbide superconductors in a filled Ti_2Ni-type structure, with remarkably high upper critical fields.[4,7]

The results presented in this paper refer to structures, crystallizing in a defect variant of the W_5Si_3-type structure, commonly known as the V_4SiSb_2 structure. The W_5Si_3 structure itself exhibits the tetragonal space group *I4/mcm*[8] and is a bulk superconductor with a critical temperature of $T_c = 2.7\,K$.[9] Other compounds crystallizing in the same structure-type and exhibiting superconducting properties are Nb_5Si_3 with a critical temperature of $T_c = 0.7$ K[10], and the ternary W_5Si_3-type compounds Nb_5Sn_2Ga, Ta_5SnGa_2, and $Zr_5Sb_{2.36}Ru_{0.36}$ with critical temperatures of $T_c \approx 1.8$ K, 1.8 K, and 5 K, respectively.[11–13]. In the V_4SiSb_2 structure, the 4*b* Wyckoff position of the W_5Si_3 structure is unoccupied, forming void channels along the *c*-direction. These channels are filled by Sb centred, essentially unhybridized 5p orbitals forming a 2D net stacking along the *c*-direction leading to "electron-filled" voids.[14] The prospect of intercalating these voids with electrophilic species has been theoretically proposed by Rytz *et al.*.[14]

To date, only six compounds have been reported to crystallize in this structure-type, namely V_4SiSb_2 and the compound series of Ti_4TBi_2 with T = Cr, Mn, Fe, Co, Ni). All of these compounds are known to be non-magnetic metals.[15,16] Furthermore, 5 pseudo-quaternary antimonides with the general formula $Nb_4Pd_{0.5}ZSb_2$ with Z = Cr, Fe, Co, Ni, Si have been reported.[17] These compounds contain three transition metals in an ordered arrangement; hence they are isostructural to each other and crystallize in substitutional variants of the W_5Si_3-type structure, or alternatively, they can be interpreted as V_4SiSb_2-type compounds with half occupied channels.

Here, we report on the discovery of the compound Nb_4SiSb_2, which crystallizes in a V_4SiSb_2-type structure with the tetragonal

[a] *Department of Quantum Matter Physics, University of Geneva, CH-1211 Geneva, Switzerland.*
[b] *Department of Chemistry, University of Zurich, CH-8057 Zurich, Switzerland.*
[c] *Department of Physics, The Hong Kong University of Science and Technology, Clear Water Bay Kowloon, Hong Kong.*
[*] *E-mail to the author*

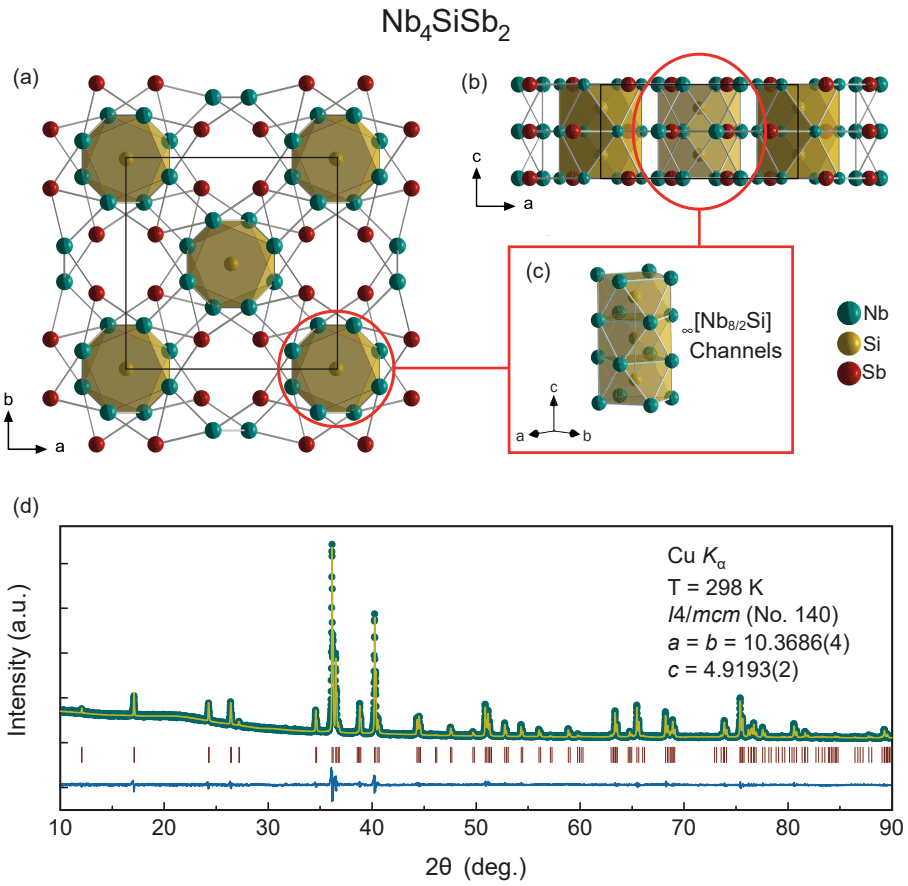

Fig. 1 Schematic representation of crystal structure obtained from SXRD refinement of Nb_4SiSb_2 along (a) the *c*-direction and (b) the *b*-direction. (c) Si − Si chains along the *c*-direction. (d) PXRD pattern of the polycrystalline sample with the respective *Rietveld* refinement. Green dots: data points, yellow line: calculated peaks, vertical dark red lines: Bragg peak positions, and the blue pattern on the bottom is the difference plot.

space group *I4/mcm*. We show that this material exhibits bulk superconductivity at a critical temperature of $T_c \approx 1.6$ K. Furthermore, we find that the 4*b* Wyckoff void position can be partially occupied by the transition metals Cu, Pd or Pt, leading to the compounds $Nb_4Cu_{0.2}SiSb_2$, $Nb_4Pd_{0.2}SiSb_2$, and $Nb_4Pt_{0.14}SiSb_2$. All three compounds are bulk superconductors with critical temperatures of $T_c \approx 1.2$ K, 0.8 K, and 0.8 K, respectively.

2 Experimental

Synthesis: Polycrystalline samples of all compounds were obtained by solid state reaction of the pressed elemental powders at high temperatures. These were synthesized using pure elements as received and stored in air of niobium (powder, 99.99%, *Alfa Aesar*), silicon (pieces, 99.95%, *Alfa Aesar*), antimony (shots, 99.999%, *Alfa Aesar*), copper (powder, 99.7%, *Merck*), palladium (powder, 99.999%, *Arcos Organics*) and platinum (powder, 99.999%, *Arcos Organics*). The elements were thoroughly mixed and ground in their stoichiometric ratios, then pressed into pellets, and subsequently sealed in quartz ampoules under 400 mbar of Ar. The quartz ampoules were heated to $T = 1100$°C with a heating rate of 180 °C/h, and annealed at this temperature for 7 days.

Diffraction: Single crystal X-ray diffraction (SXRD) data were collected at $T = 160(1)\,K$ on a *Rigaku* XtaLAB Synergy, Dualflex, Pilatus 200K diffractometer using a monochromatic X-ray source (Cu K_{α_1} radiation: $\lambda = 1.54184$ Å) from a micro-focus sealed X-ray tube and cooled using an *Oxford* liquid-nitrogen Cryostream device. The selected suitable single crystals were mounted using polybutene oil. Pre-experiment, data collection, data reduction and analytical absorption correction[18] were performed with the program suite CrysAlisPro. Using Olex2[19], the structure was solved with the SHELXT[20] small molecule structure solution program and refined with the SHELXL2018/3 program package[21] by full-matrix least-squares minimization on F2. PLATON[22] was used to check the result of the X-ray analysis. CCDC 2166026 (for $Nb_4Cu_{0.2}SiSb_2$), 2166027 (for $Nb_4Pd_{0.2}SiSb_2$), 2166028 (for $Nb_4Pt_{0.14}SiSb_2$) and 2166029 (for Nb_4SiSb_2) contain the supplementary crystallographic data for these compounds, and can be obtained free of charge from the Cambridge Crystallographic Data Centre via www.ccdc.cam.ac.uk/data_request/cif.

Powder X-ray diffraction (PXRD) measurements were performed on a *Rigaku* SmartLab diffractometer using a Cu X-ray source ($K_{\alpha 1} = 1.540600$ Å, $K_{\alpha 2} = 1.544430$ Å) with CuK_β filter and collected using a 2θ range of 5–100°. The machine is equipped with a 3 kW sealed X-ray tube, CBO optics and a D/teX Ultra 250 silicon strip detector. Data was recorded using the *SmartLab* Stu-

dio II software. *Rietveld* refinements were performed using the *FULLPROF* software package[23] and fitting of the diffracted data was done using the *Thompson-Cox-Hastings* pseudo-*Voigt* function with asymmetry correction.[24]

Physical Properties: Physical property measurements were carried out on sintered, flat pellets. Temperature-dependent resistivity measurements were performed with a Quantum Design Physical Property Measurement System (PPMS) using a He-3 insert for temperature measurements down to 500 mK. A four-point resistivity measurement method, using silver wires ($50\,\mu m$ diameter) was employed.

Specific heat measurements were performed from 300 mK to 2 K in a He-3 15 T magnet cryostat with a custom-developed modulated-temperature AC calorimetry technique using an SR830 digital lock-in amplifier, and from 2 - 10 K with a long relaxation technique in a He-4 cryostat. For the latter, each relaxation provides about 1000 data points over a temperature interval of 30-40% of the base temperature, which has been varied between 2 K and 10 K. The relaxation technique provides a high precision up to 1% while the AC technique is less accurate but provides high resolutions of $\Delta C/C$ of 10^{-5} at a high density of data points.[25] Temperature-dependent magnetization measurements were performed using a Quantum Design Magnetic Properties Measurement System (MPMSXL) equipped with a reciprocating sample option (RSO) and a 7 T magnet.

3 Results and Discussion

3.1 Crystal Structure of Nb_4SiSb_2

In Figure 1a and b, we present the crystal structure and the unit cell of the single-crystal refinement of Nb_4SiSb_2, shown along the *c*-direction and along the *b*-direction, respectively. The structure of Nb_4SiSb_2 was determined by means of single crystal X-Ray diffraction (SXRD) at 160 K and the elemental composition was confirmed using EDX analysis at ambient temperature (Supplementary Information).

We find Nb_4SiSb_2 to crystallize in the tetragonal space group *I4/mcm* with the lattice parameters $a = b = 10.3638(2)$ Å and $c = 4.9151(2)$ Å with the corresponding calculated cell volume of $V = 527.92(3)$ Å^3. Hence, it is found to adopt the same centrosymmetric structure type that was previously reported for V_4SiSb_2[15,16]. The crystallographic data and the details of the structure refinement are summarised in Table 1. All crystallographic positions as well as the anisotropic displacement parameters are presented in Table 2.

In the structure of Nb_4SiSb_2 each atom occupies one atomic site: The niobium atoms are located at the 16*k* *Wyckoff* position, silicon occupies the 4*a* and antimony the 8*h* *Wyckoff* positions. Silicon forms thereby columns which can be interpreted as $_\infty[Nb_{8/2}Si]$ chains along the *c*-direction as shown in Figure 1(c). The Si–Si bonding distance in Nb_4SiSb_2 within the columns is 2.4576(1) Å, which is in good agreement with the ones found in V_4SiSb_2[15] and comparable to Si–Si bond distances in similar structures.[17,26] Each Si atom is surrounded by eight Nb atoms with a distance of 2.6252(6) Å forming antiprisms with the surrounding neighbour atoms. Nb has a coordination number (CN) of 13 consisting of six Nb neighbours located in the $_\infty[Nb_{8/2}Si]$ column, one Nb in the adjacent $_\infty[Nb_{8/2}Si]$ column, two Si, and four Sb neighbours located in between the two columns. The Nb–Nb distances range from 3.0275(8) to 3.2807(9) Å. These distances, together with the relatively short intercolumn distance between two Nb atoms of 3.0449(13) Å are in good agreement with distances found in comparable structures.[27,28] Also, the Nb–Sb distance ranging from 2.8238(7) Å to 2.9781(4) Å is in good agreement with the distances found in the related compounds, such as e.g. in Nb_5Sb_4.[28] Each Sb has eight Nb neighbours and therefore a CN of 8. Another feature of this structure are the voids at the 4*b* *Wyckoff* position. These void positions are surrounded by four Sb atoms. These form void channels along the *c*-direction. If these void positions were fully occupied, then the V_4SiSb_2 structure would be equivalent to the W_5Si_3 structure.[15]

The validity of the structural model, the phase purity, and the homogeneity of the sample were confirmed by means of PXRD at ambient temperature and SXRD at 160 K. The reliability factors of the SXRD refinement can be found in the supplementary information. In figure 3(d) the PXRD pattern of the polycrystalline sample is shown, with its respective *Rietveld* refinement. We find the lattice parameters of $a = b = 10.3686(4)$ Å , and $c = 4.9193(2)$ Å , as well as a calculated cell volume of $V = 528.86(3)$ Å^3. Hence, the SXRD and PXRD refinements and structural solutions are in excellent agreement with each other (Supplementary Information).

3.2 Superconducting Properties of Nb_4SiSb_2

In Figure 2(a), we show the temperature-dependant resistivity of Nb_4SiSb_2 in zero field $\mu_0 H = 0\,T$ as $\rho(T)$ between T = 300 K and 500 mK (inset) and in the vicinity of the superconducting transition. A sharp drop in the resistivity is observed at low temperature, corresponding to a transition to a superconducting state. The transition midpoint of $T_{c,mid} \approx 1.65$ K and reaches a state of zero resistance at $T_{zero} \approx 1.56$ K. The transition is comparably sharp with a transition width of $\Delta T = 0.18$ K in the resistivity. The residual resistivity $\rho(1.8\text{ K}) = 0.14\,\text{m}\Omega$ cm at 1.8 K and the room temperature resistivity value of $\rho(300\text{ K}) = 2.06\,\text{m}\Omega$ cm, result in a residual resistivity ratio (RRR) here defined as RRR $= \rho(300K)/\rho(1.8K) = 14.96$. This RRR value corresponds to the value of a good metal.

The bulk nature of the superconductivity in Nb_4SiSb_2 is confirmed by low-temperature specific-heat measurements. Temperature-dependent specific-heat measurements are of particular importance to prove the bulk nature of a superconductor.[29,30]

In Figure 2(b), we present the temperature-dependent specific heat $C(T)/T$ of Nb_4SiSb_2 in a temperature range between $T =$ 600 mK and 2 K. We find a clearly pronounced discontinuity in the specific heat, resulting from the superconducting transition. The data was fitted using the α-model.[31,32] Thereby, an entropy conserving construction was used to determine the critical temperature, $T_c \approx 1.6$ K. This value is in good agreement with the critical temperature from the resistivity measurement. From the α-model fit, we obtained $\alpha = 1.7$ and the Sommerfeld constant

Table 1 Details of the SXRD measurements and structural refinements for Nb_4SiSb_2, $Nb_4Cu_{0.2}SiSb_2$, $Nb_4Pd_{0.2}SiSb_2$ and $Nb_4Pt_{0.14}SiSb_2$

Parameters	Nb_4SiSb_2	$Nb_4Cu_{0.2}SiSb_2$	$Nb_4Pd_{0.2}SiSb_2$	$Nb_4Pt_{0.14}SiSb_2$
Crystal system	tetragonal	tetragonal	tetragonal	tetragonal
Structure-type	V_4SiSb_2	W_5Si_3(defect)	W_5Si_3(defect)	W_5Si_3(defect)
Space group	*I4/mcm* (No. 140)	*I4/mcm* (No. 140)	*I4/mcm* (No. 140)	*I4/mcm* (No. 140)
Absorption correction method	analytical	analytical	spherical	analytical
Temperature [K]	160(1)	160(1)	160(1)	160(1)
Lattice parameters [Å]	a = 10.3638(2) c = 4.9151(2)	a = 10.3954(2) c = 4.9233(2)	a = 10.3991(2) c = 4.93619(16)	a = 10.3803(2) c = 4.9348(2)
Cell volume [Å^3]	527.92(3)	532.03(3)	533.81(3)	531.73(3)
Formula unit/cell	4	4	4	4
ρ_{calcd} [g cm^{-3}]	8.093	8.189	8.268	8.376
μ [mm^{-1}]	149.393	532.03(3)	153.021	155.001
Crystal size [mm]	0.018 x 0.016 x 0.013	0.005 x 0.003 x 0.002	0.01 x 0.01 x 0.01	0.015 x 0.015 x 0.01
F(000)	1120.0	1143.0	1157.0	1164.0
Radiation type	Cu K_α (λ = 1.54184)	Cu K_α (λ = 1.54184)	Cu K_α (λ = 1.54184)	Cu K_α (λ = 1.54184)
2 Θ range [°]	12.078 to 146.58	12.04 to 148.58	12.036 to 147.576	12.058 to 147.716
Index range	h[-9,12] k[-12,12] l[-5,6]	h[-11,9] k[-12,12] l[-6,6]	h[-11,12] k[-12,12] l[-6,5]	h[-12,12] k[-12,12] l [-6,5]
Observed reflections	1466	838	2368	2381
Independent reflections (2 σ)	165	166	166	167
R_{int}	0.0278	0.0385	0.0312	0.0298
R_σ	0.0127	0.0314	0.0107	0.0117
Refined parameters	14	16	16	17
GOF	1.363	1.142	1.252	1.240
R_1 (all data) (%)	1.69	3.33	1.64	1.60
wR_1 ($\geq 2\sigma$) (%)	1.69	2.96	1.62	1.57
wR_2 (all data) (%)	4.32	7.53	3.71	3.67
wR_2 ($\geq 2\sigma$) (%)	4.33	7.37	3.71	3.66
Max/min residual electron density [e Å^{-3}]	1.41/-0.94	1.12/-1.52	0.97/-0.98	1.13/-0.85

Table 2 Atomic coordinates, occupancy, isotropic and anisotropic displacement parameters of the SXRD refinements at 160 K under atmospheric pressure for the compounds Nb_4SiSb_2, $Nb_4Cu_{0.2}SiSb_2$, $Nb_4Pd_{0.2}SiSb_2$ and $Nb_4Pt_{0.14}SiSb_2$ (Space Group *I*4/*mcm*, No. 140)

Nb_4SiSb_2									
Atom	*Wyckoff* Symbol	*x*	*y*	*z*	U(eq) [Å^2]	U_{11} / U_{22}	U_{33}	U_{12}	Occ.
Nb	16*k*	0.29305(6)	0.58530(6)	1/2	0.0111(3)	10.6(4) / 10.9(4)	11.8(4)	0.2(2)	4.00
Si	4*a*	1/2	1/2	3/4	0.0122(3)	10.1(11) / 10.1(11)	16(2)	0	1.00
Sb	8*h*	0.14037(5)	0.35963(5)	1/2	0.0119(9)	11.8(3) / 11.8(3)	13.0(5)	-1.5(3)	2.00
$Nb_4Cu_{0.2}SiSb_2$									
Atom	*Wyckoff* Symbol	*x*	*y*	*z*	U(eq) [Å^2]	U_{11} / U_{22}	U_{33}	U_{12}	Occ.
Nb	16*k*	0.29297(9)	0.41603(9)	1/2	0.0080(4)	6.2(6) / 6.4(6)	11.4(6)	0.3(4)	4.00
Cu	4*b*	0	1/2	3/2	0.021(7)	24(8) / 24(8)	16(12)	0	0.199(16)
Si	4*a*	1/2	1/2	3/2	0.0063(12)	3.2(17) / 3.2(17)	12(3)	0	1.00
Sb	8*h*	0.14385(8)	0.35615(2)	1/2	0.0110(4)	8.8(5) / 8.8(5)	15.3(7)	2.3(4)	2.00
$Nb_4Pd_{0.2}SiSb_2$									
Atom	*Wyckoff* Symbol	*x*	*y*	*z*	U(eq) [Å^2]	U_{11} / U_{22}	U_{33}	U_{12}	Occ.
Nb	16*k*	0.29305(4)	0.58369(4)	1/2	0.0125(2)	12.1(3) / 12.8(3)	12.7(3)	-0.01(17)	4.00
Pd	4*b*	0	1/2	1/4	0.0147(15)	13.6(16) / 13.6(16)	17(2)	0	0.199(5)
Si	4*a*	1/2	1/2	3/2	0.0131(6)	13.1(8) / 13.1(8)	13.0(14)	0	1.00
Sb	8*h*	0.14470(4)	0.35530(4)	1/2	0.0170(2)	15.8(2) / 15.8(2)	19.5(3)	-3.5(2)	2.00
$Nb_4Pt_{0.14}SiSb_2$									
Atom	*Wyckoff* Symbol	*x*	*y*	*z*	U(eq) [Å^2]	U_{11} / U_{22}	U_{33}	U_{12}	Occ.
Nb	16*k*	0.58429(5)	0.29284(5)	1/2	0.0063(2)	6.3(3) / 6.2(3)	6.5(4)	-0.08(18)	4.00
Pt	4*b*	1/2	0	3/2	0.0122(5)	12.5(17) / 12.5(17)	12(3)	0	0.140(3)
Si	4*a*	1/2	1/2	3/2	0.0020(6)	2.7(8) / 2.7(8)	0.7(16)	0	1.00
Sb	8*h*	0.35697(4)	0.14303(4)	1/2	0.0101(3)	9.0(3) / 9.0(3)	12.5(4)	-3.1(2)	2.00

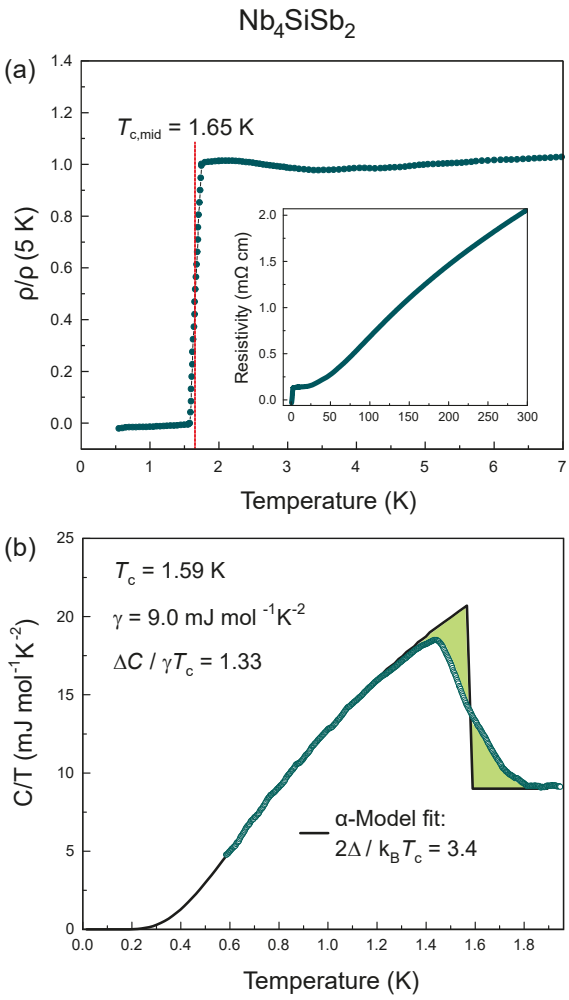

Fig. 2 (a) normalized, low-temperature resistivity of Nb_4SiSb_2 in a temperature range between $T = 500$ mK and 5 K measured in zero field $\mu_0 H = 0T$. Inset: Temperature-dependant resistivity of Nb_4SiSb_2 in zero field $\mu_0 H = 0T$ as $\rho(T)$ between T = 500 mK and 300 K (b) Specific heat capacity of Nb_4SiSb_2 in a temperature range between $T = 580$ mK and 2 K. The black line corresponds to a fit using the α-model.

of $\gamma = 9.00$ mJ mol^{-1} K^{-2}. We find a ratio for the normalized specific-heat jump of Δ C/ γ T_c = 1.33 mJ mol^{-1} K^{-2}, which confirms the bulk nature of the superconductivity, as this value is close to the weak-coupling BCS ratio of 1.43. This corresponds to a value of the superconducting gap of $2\Delta(0) = 3.4 k_B T_c$.

Under the assumption of a degenerate electron gas of non-interacting particles, the electronic contribution to the heat capacity in a solid at low temperatures is proportional to the density of states at the *Fermi* level $D(E_F)$ and linear in T. With the previously determined value of $\gamma = 9.00$ mJ mol^{-1} K^{-2}, the density of states at the *Fermi* level can be calculated as described by *F. Heiniger et al.*[33] according to

$$C_{el} = \gamma T = \frac{\pi^2}{3} k_B^2 D(E_F) T. \quad (1)$$

We obtain for Nb_4SiSb_2 a density of states at the *Fermi* level of $D(E_F) = 3.8$ states eV^{-1}.

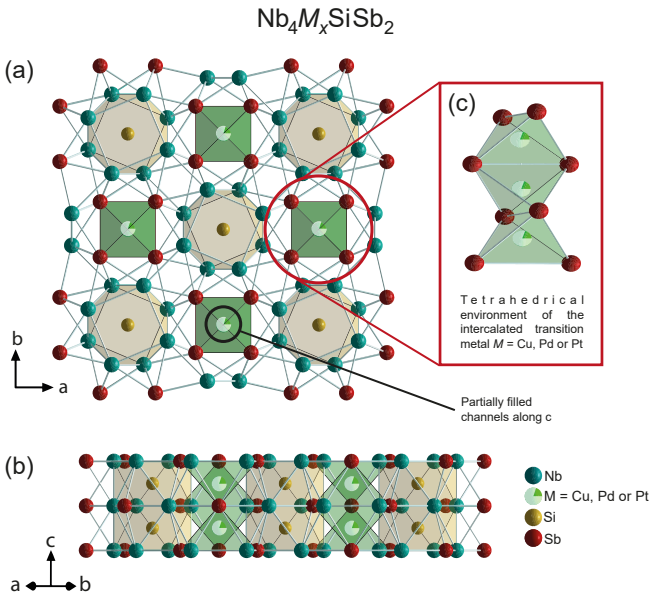

Fig. 3 Schematic representation of the structures of $Nb_4M_xSiSb_2$ from (a) the *c*-direction and (b) a high symmetry-direction. (c) illustrates the intercalated transition metal *M* (Cu, Pd, or Pt) in its environment within the $_\infty[Sb_{4/2}M_x]$ channels. The crystal structures were obtained from SXRD refinements.

Magnetic susceptibility measurements of Nb_4SiSb_2 were conducted in the normal-state, i.e. in a temperature range between $T = 10$ K to 300 K, in an external field of $\mu_0 H = 1$ T. The observed temperature-independent positive magnetic moment corresponds to a *Pauli*-paramagnet (see Supplementary Information). A summary of all obtained physical parameters can be found in Table 3.

3.3 Crystal Structures of $Nb_4Cu_{0.2}SiSb_2$, $Nb_4Pd_{0.2}SiSb_2$, and $Nb_4Pt_{0.14}SiSb_2$

We have synthesized the three compounds $Nb_4Cu_{0.2}SiSb_2$, $Nb_4Pd_{0.2}SiSb_2$, and $Nb_4Pt_{0.14}SiSb_2$. Here, the void 4*b* Wyckoff positions in Nb_4SiSb_2 are partially filled with a transition metal M = Cu, Pd, or Pt, respectively. In Figure 3, we show a schematic representation of the unit cell along the *c*-direction and a high symmetry-direction of $Nb_4M_xSiSb_2$, where M = Cu, Pt and Pd with x = 0.2, 0.14 and 0.2. The crystal structures of all three compounds were determined using SXRD at 160 K and PXRD diffraction at room temperature.

All samples were found to be single phase by means of PXRD measurements and corresponding Rietveld refinements (Supplementary Information). Atomic compositions were confirmed using EDX analysis (Supplementary Information).

All three structures are in good agreement with the previously reported structure for $Nb_4Pd_{0.5}ZSb_2$ with Z = Cr, Fe, Co, Ni, Si, where it was thought that a half-occupied Pd 4*b* site was necessary to stabilize these compounds.[17] In contrary to this previous assumption, we found here that the channels were in our case either unoccupied or filled with 0.2 or 0.14 respectively (in case of Pt), independent of the initially used starting stoichiometry. These results indicate that, with improved synthesis methodolo-

Table 3 Summary of the physical parameters for Nb_4SiSb_2, $Nb_4Cu_{0.2}SiSb_2$, $Nb_4Pd_{0.2}SiSb_2$ and $Nb_4Pt_{0.14}SiSb_2$

Parameter	Units	Nb_4SiSb_2	$Nb_4Cu_{0.2}SiSb_2$	$Nb_4Pd_{0.2}SiSb_2$	$Nb_4Pt_{0.14}SiSb_2$
$T_{c,resistivity}$	K	1.65	1.16	0.76	0.84
$T_{c,specificheat}$	K	1.59	-	-	-
RRR	-	14.96	4.54	1.56	1.70
$\rho(300)$	mJ Ω cm	2.06	0.70	8.46	2.49
ρ_0	mJ Ω cm	0.13	0.15	5.43	1.46
Type of magnetism	-	*Pauli*-paramagnetic	*Pauli*-paramagnetic	*Pauli*-paramagnetic	*Pauli*-paramagnetic
γ	mJ mol^{-1} K^{-2}	9.00	7.5	-	
$\Delta C/T_c\gamma$	-	1.33	1.2	-	
$2\Delta(0)$	meV	0.47	12	-	
$D(E_F)$	states eV^{-1} per f.u.	3.82	3.18	-	

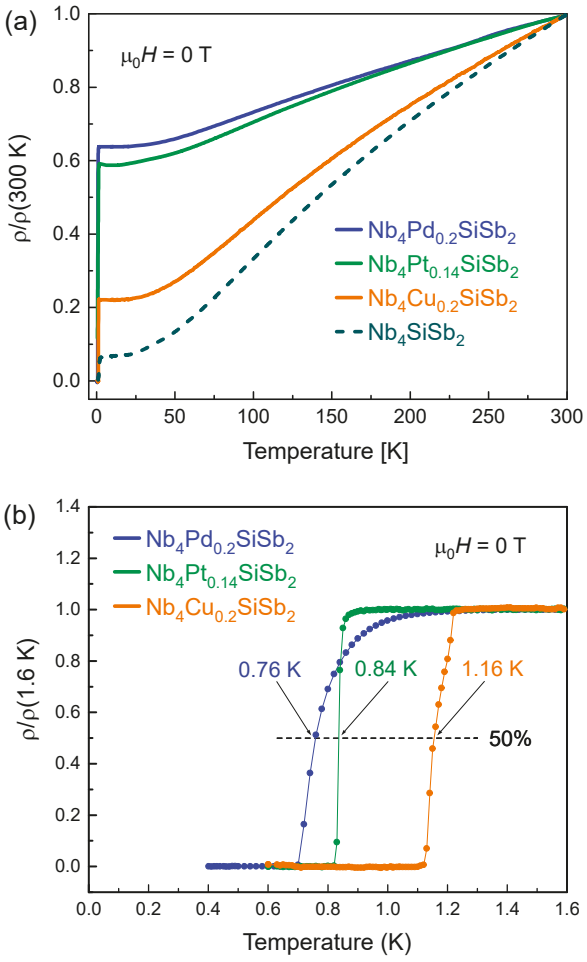

Fig. 4 (a) Temperature-dependent resistivity of $Nb_4Cu_{0.2}SiSb_2$, $Nb_4Pd_{0.2}SiSb_2$ and $Nb_4Pt_{0.14}SiSb_2$ (a) over the whole temperature range between T = 400 mK and 300 K, and (b) in the vicinity of the superconducting transitions at low temperatures. All measurements were performed in zero field $\mu_0 H = 0T$.

gies, the continuous solid solution might be accessible in the future. All information regarding the lattice parameters, crystallographic data, and details of the structure refinements are summarized in Table 1.

3.4 Electronic Properties of $Nb_4Cu_{0.2}SiSb_2$, $Nb_4Pd_{0.2}SiSb_2$ and $Nb_4Pt_{0.14}SiSb_2$

In Figure 4 we present the temperature-dependent resistivity and the normalized low-temperature resistivity $\rho(T)/\rho(1.6K)$ in a temperature range between T = 400 mK and 1.6 K for $Nb_4Cu_{0.2}SiSb_2$, $Nb_4Pd_{0.2}SiSb_2$ and $Nb_4Pt_{0.14}SiSb_2$, measured in zero field $\mu_0 H = 0T$.

We find all three compounds to undergo a transition to a superconducting state at low temperatures. The critical temperature midpoints are determined as $T_{c,mid} \approx 1.16$ K for $Nb_4Cu_{0.2}SiSb_2$, $T_{c,mid} \approx 0.76$ K for $Nb_4Pd_{0.2}SiSb_2$ and $T_{c,mid} \approx 0.84$ K for $Nb_4Pt_{0.14}SiSb_2$. All three compounds with atoms in the void position of Nb_4SiSb_2 have lower transition temperatures than the parent compound.

For comparison, we have performed specific heat measurements in the normal state of Nb_4SiSb_2 and $Nb_4Pt_{0.14}SiSb_2$ (shown in the SI). For Nb_4SiSb_2 we find values for γ_n and β of 8.40 mJ mol^{-1} K^{-2} and 0.16 mJ mol^{-1} K^{-4}, respectively. The γ_n value of this fit is in good agreement with the more accurate low-temperature value discussed above. For $Nb_4Pt_{0.14}SiSb_2$ we find values for γ_n and β of 9.10 mJ mol^{-1} K^{-2} and 0.31 mJ mol^{-1} K^{-4}, respectively. We note that the values for γ_n differ only slightly, indicating a small change of the electronic properties upon void position filling. We find, however, that β changes quite strongly. These findings indicate that the decrease of the superconducting transition temperature is likely caused by a change in the phonons, and the vibrations, respectively.

$Nb_4Pd_{0.2}SiSb_2$ has the lowest critical temperature of the doped compounds, as well as the lowest RRR value of RRR = $\rho(300K)/\rho(1.8K) = 1.56$. $Nb_4Cu_{0.2}SiSb_2$ with RRR = 4.54 and $Nb_4Pt_{0.14}SiSb_2$ with RRR = 1.70 follow the descending trend observed for the critical temperatures accordingly. These low RRR values correspond to a poor metallic behaviour and are 3 to 24 times smaller than the RRR of the parent compound Nb_4SiSb_2. The pronounced effect on the physical properties on void position doping becomes clearly apparent in the large change of the RRR values. The nature of the change is, however, not only affected by the electronic states, but also by the phonons and by impurity state scattering.

4 Conclusion

We have reported on the discovery of the centrosymmetric structure compound Nb_4SiSb_2. This phase was found to crystallize in the tetragonal V_4SiSb_2-type structure. We found Nb_4SiSb_2 to undergo a transition to a superconducting state at a critical temperature of $T_c \approx 1.6K$. The bulk nature of the superconducting transition was evidenced by a clear discontinuity in specific heat, with a normalized specific heat jump of $\Delta C(T_c)/\gamma T_c = 1.33$ mJ mol^{-1} K^{-2}, close to the weak-coupling BCS value. Furthermore, we have shown that the unoccupied 4*b* Wyckoff site in Nb_4SiSb_2 can be partially occupied with the transition metals Cu, Pd, or Pt.

These compounds crystallize in a tetragonal variant of the W_5Si_3-type structure with partially occupied channels, extending along the *c*-direction. All three compounds were found to be superconductors with transitions temperatures of $T_c \approx 1.2K$ for $Nb_4Cu_{0.2}SiSb_2$, $T_c \approx 0.8K$ for $Nb_4Pd_{0.2}SiSb_2$ and $T_c \approx 0.8K$ for $Nb_4Pt_{0.14}SiSb_2$. We find that the insertion of a host atom into the void positions strongly affects the electronic and superconducting properties of this material.

Hence, our results indicate that this and related compounds might be promising host structures for the discovery of new superconducting materials, as they allow for a controlled manipulation of the electronic and phononic properties by chemical manipulation.

Conflicts of Interest

There are no conflicts to declare.

Acknowledgements

This work was supported by the Swiss National Science Foundation under Grant No. PCEFP2_194183 and by grants from the Research Grants Council of the Hong Kong Special Administrative Region, China (GRF-16302018 & C6025-19G-A).

Notes and references

1 D. Yazici, K. Huang, B. D. White, I. Jeon, V. W. Burnett, A. J. Friedman, I. K. Lum, M. Nallaiyan, S. Spagna and M. B. Maple, *Phys. Rev. B - Condens. Matter Mater. Phys.*, 2013, **B 87**, 1–8.

2 Y. Zhang, B. Wang, Z. Xiao, Y. Lu, T. Kamiya, Y. Uwatoko, H. Kageyama and H. Hosono, *npj Quantum Mater.*, 2017, **2**, 45.

3 J. Akimitsu, *Proc. Jpn. Acad. Ser. B Phys. Biol. Sci.*, 2019, **95**, 321–342.

4 K. Ma, K. Gornicka, R. Lefèvre, Y. Yang, H. M. Rønnow, H. O. Jeschke, T. Klimczuk and F. O. von Rohr, *ACS Mater. Au*, 2021, **1**, 55–61.

5 B. Wang, Y. Zhang, S. Xu, K. Ishigaki, K. Matsubayashi, J.-G. Cheng, H. Hosono and Y. Uwatoko, *Chin. Physics B*, 2019, **28**, 107401.

6 A. D. Bortolozo, C. A. Dos Santos, R. F. Jardim, C. Ritter, A. Devishvili, M. Rotter, F. G. Gandra and A. J. MacHado, *J. Appl. Phys.*, 2012, **111**, 1–6.

7 K. Ma, R. Lefèvre, K. Gornicka, H. O. Jeschke, X. Zhang, Z. Guguchia, T. Klimczuk and F. O. von Rohr, *Chem. Mater.*, 2021, **33**, 8722–8732.

8 B. Aronsson, O. Tjomsland, R. Lundén and H. Prydz, *Acta Chem. Scand.*, 1955, **9**, 1107–1110.

9 K. Kawashima, T. Muranaka, Y. Kousaka, S. Akutagawa and J. Akimitsu, *J. Phys. Conf. Ser.*, 2009, **150**, 1–4.

10 J. O. Willis, *J. Appl. Phys.*, 1979, **50**, 2863–2865.

11 T. Shishido, K. Ukei, N. Toyota, T. Sasaki, Y. Watanabe, K. Motai, T. Fukuda, H. Takeya and H. Takei, *J. Cryst. Growth*, 1989, **96**, 1–6.

12 T. Shishido, J. Ye, N. Toyota, K. Ukei, T. Sasaki, H. Horiuchi and T. Fukuda, *Jpn. J. Appl. Phys.*, 1989, **28**, 1519–1520.

13 W. Xie, H. Luo, B. F. Phelan and R. J. Cava, *J. Mater. Chem. C*, 2015, **3**, 8235–8240.

14 R. Rytz and R. Hoffmann, *Inorg. Chem.*, 1999, **38**, 1609–1617.

15 P. Wollesen and W. Jeitschko, *J. Alloys Compd.*, 1996, **243**, 67–69.

16 G. C. Richter, W. Jeitschko, B. Künnen and H. M. Gerdes, *Inorg. Chem.*, 1997, **133**, 400–406.

17 M. Wang, W. C. Sheets, R. McDonald and A. Mar, *Inorg. Chem.*, 2001, **40**, 5199–5205.

18 R. Clark and J. Reid, *Acta Crystallographica Section A: Foundations of Crystallography*, 1995, **51**, 887–897.

19 O. V. Dolomanov, L. J. Bourhis, R. J. Gildea, J. A. Howard and H. Puschmann, *Journal of applied crystallography*, 2009, **42**, 339–341.

20 G. M. Sheldrick, *Acta Crystallographica Section A: Foundations and Advances*, 2015, **71**, 3–8.

21 G. M. Sheldrick, *Acta Crystallographica Section C: Structural Chemistry*, 2015, **71**, 3–8.

22 A. L. Spek, *Acta Crystallographica Section D: Biological Crystallography*, 2009, **65**, 148–155.

23 J. Rodríguez-Carvajal, *Physica B: Condensed Matter*, 1993, **192**, 55–69.

24 L. Finger, D. Cox and A. Jephcoat, *Journal of applied Crystallography*, 1994, **27**, 892–900.

25 H. K. Mak, P. Burger, L. Cevey, T. Wolf, C. Meingast and R. Lortz, *Phys. Rev. B Condens. Matter*, 2013, **87**, 214523.

26 M. E. Badding and F. J. DiSalvo, *Inorg. Chem.*, 1990, **29**, 3952–3954.

27 S. Janger and S. E. Rasmussen, *Acta Crystallogr.*, 1975, **B31**, 2881 – 2883.

28 Y. F. Lomnytska and Y. B. Kuz'ma, *J. Alloys Compd.*, 2006, **413**, 114–117.

29 E. M. Carnicom, W. Xie, Z. Yang, K. Górnicka, T. Kong, T. Klimczuk and R. J. Cava, *Chem. Mater.*, 2019, **31**, 2164–2173.

30 C. Witteveen, K. Górnicka, J. Chang, M. Månsson, T. Klimczuk and F. O. von Rohr, *Dalt. Trans.*, 2021, **50**, 3216–3223.

31 H. Padamsee, J. E. Neighbor and C. A. Shiffman, *J. Low Temp. Phys.*, 1973, **12**, 387–411.

32 D. C. Johnston, *Supercond. Sci. Technol.*, 2013, **26**, 1–19.

33 F. Heiniger, E. Bucher and J. Muller, *Phys. der Kondens. Mater.*, 1966, **5**, 243–284.